COMPUTATIONS OF ROTORCRAFT AEROACOUSTICS WITH A NAVIER-STOKES/KIRCHHOFF METHOD

Jasim Ahmad
Sterling Software, NASA Ames Research Center, Moffett Field, CA

Earl P. N. Duque & Roger C. Strawn
US Army Aeroflightdynamics Directorate, ATCOM, Ames Research Center, Moffett Field, CA

Abstract

This paper describes a new method for computing the flowfield and acoustic signature of arbitrary rotors in forward flight. The overall scheme uses a finite-difference Navier-Stokes solver to compute the aerodynamic flowfield near the rotor blades. The equations are solved on a system of overset grids that allow for prescribed cyclic and flapping blade motions and capture the interactions between the rotor blades and wake. The far-field noise is computed with a Kirchhoff integration over a surface that completely encloses the rotor blades. Flowfield data are interpolated onto this Kirchhoff surface using the same overset-grid techniques that are used for the flowfield solution. As a demonstration of the overall prediction scheme, we compare computed and experimental far-field noise results in cases with high-speed impulsive (HSI) and blade-vortex interaction (BVI) noise. Computed HSI results show better agreement with experiment than BVI results and it is clear that the Navier-Stokes flow solver requires improved grid resolution in the rotor wake to capture the details of BVI noise. Overall, the overset-grid CFD scheme provides a powerful new framework for the prediction of rotorcraft noise

Introduction

Modern helicopter designs aim for low noise and this is particularly true for civilian helicopters that operate near heavily populated areas. There are two main types of noise that cause problems for helicopters. The first is called high-speed impulsive (HSI) noise and consists of a strong acoustic disturbance occurring over a short period of time. Impulsive noise is generally associated with high tip speeds and advancing-tip Mach numbers greater than 0.9. The second type of noise comes from the interaction of the rotor blades with their vortical wake systems. This type of noise is called blade-vortex interaction (BVI) noise and it is particularly important when the helicopter is descending for landings.

Accurate prediction of both types of rotor noise is heavily dependent on the accurate prediction of the aerodynamic flowfield around the rotor blades. Tip vortices in the rotor wake dominate the flowfield and produce a highly unsteady and nonuniform induced velocity field at the rotor disk. The rotor wake is very difficult to model but holds the key to accurate acoustic predictions.

Flowfield models based on computational fluid dynamics (CFD) hold a great deal of promise for simulating the aerodynamics of helicopter rotors and their wake systems. The rotor wake can be captured directly without ad-hoc models and the nonlinear flowfield close to the rotor blades is modeled accurately. Overset grid schemes allow for efficient placement of grids around complicated geometries and also provide a framework for solution adaption and future improvements in the resolution of the wake system.

The CFD solutions in this paper use the overset grid method for helicopter aerodynamics that was developed by Ahmad and Duque[1]. The method includes a user-prescribed motion of the blade that models the effects of cyclic pitch control and rotor blade flapping. The interactions between the rotor blades and their wake systems are captured as an integral part of the CFD solution. References [2-4] provide additional examples of overset-grid CFD methods for helicopter aerodynamics.

Even if the flowfield near the rotor blade is computed accurately with a CFD model, it is not practical to extend this CFD solution to compute the helicopter acoustics in the far field. Away from the rotor blades, more efficient Kirchhoff methods for acoustic propagation can be used that are based on linear theory. This type of combined solution method is a good compromise between efficiency and accuracy. The CFD equations model the nonlinear effects near the rotor blade surfaces and the linear Kirchhoff methods propagate the acoustic signal to the far field in a computationally-efficient manner.

The Kirchhoff method computes the acoustic pressure in the far field from a numerical integration over a surface that completely encloses the rotor blades. Aerodynamic and acoustic solutions in the near field are computed with an appropriate CFD method and interpolated onto the Kirchhoff surface using overset-grid interpolation tools and then stored for acoustic postprocessing. The Kirchhoff acoustics prediction scheme from Strawn et al. [5-7] is

---

Presented at the 22nd European Rotorcraft Forum, Brighton, UK, 17-19 Sept. 1996.

used in this paper. It is specifically developed for compatibility with overset grid systems and previous results with this scheme have compared very well with experimental data for both HSI and BVI noise.

The overall Navier-Stokes/Kirchhoff (NS/Kirchhoff) scheme described in this paper was first presented in Ref. [8]. However, the results for this paper are significantly different from those of Ref. [8] due to the correction of several errors in the test-case setups and postprocessing. Also, the present computations use 3rd order accurate spatial differencing as opposed to 2nd order in Ref. [8].

The combination of CFD solutions near the rotor blade with Kirchhoff methods for the far-field offers high accuracy with reasonable computer resource requirements. By incorporating the Kirchhoff surface into the existing framework for overset-grid CFD solvers, we can compute the far-field acoustics solution with very little additional cost compared to the CFD solution alone.

The main purpose of this paper is to present the framework for our new combined aeroacoustics prediction method. Computed results for HSI and BVI noise are still preliminary and will improve as we fine-tune individual parts of the overall scheme.

CFD Methodology

Algorithm

The main flow solver is based upon the OVERFLOW1.6ap code by Buning, et.al. [9]. OVERFLOW 1.6ap is a general purpose Navier-Stokes code for static grid type computations. Meakin [3] used an earlier version of the OVERFLOW code and coupled his domain connectivity algorithm (DCF) to the solver. Ahmad and Duque [1] used the same connectivity algorithm with a different flow solver and included the modeling of arbitrary rigid blade motion. In our current work, the generality of the OVERFLOW code is combined with the dynamic grid capability of DCF and user-specified rigid blade motion.

The OVERFLOW code has a number of available flow solvers such as the block Beam-Warming scheme. However, stability constraints severely limit the timesteps for this scheme. Srinivasan et al. [10] showed that one can use larger time steps and achieve adequate solution accuracy by using the implicit LU-SGS method by Yoon [11] along with Roe upwinding. The flux terms use a Roe upwind-biased scheme for all three coordinate directions with higher-order MUSCL-type limiting to model shocks accurately [12]. The resulting method then is third-order accurate in space and first-order accurate in time. The OVERFLOW code now has the LU-SGS method as a solver option along with 3rd order Roe upwinding.

The OVERFLOW code was designed to take full advantage of overset grid systems which simplify the grid generation for complicated geometries and bodies in relative motion. For instance, the aerodynamic near-field can be modeled by one or more grids that are attached to the moving rotor blades. These rotating grids move through, and are enclosed by, a nonrotating background grid that captures the rotor wake. The flowfield equations are solved on each grid in an alternating sequence, with interpolated boundary information passed back and forth between each grid.

Domain Connectivity Functions

Interpolations between overset grids can be explained by noting that, during the grid motions, a portion of the background grid lies within the interior of the rotor blades. When this situation occurs, these points must be removed from the flow solver, creating "holes". Removal of the hole regions from the background grid creates a set of boundary points known as hole fringe points. The near-field rotor-blade grids interpolate data to the background grid at the background grid's hole fringe points. Similarly, the background grid interpolates data to the outer boundaries of the rotor grid, which is typically 2 or 3 chordlengths away from the rotor surface.

With moving overset grids, their overlap boundaries, or connectivities, change with time. We use a computer code known as DCF3D (Domain Connectivity Functions in Three Dimensions) to determine the changing connectivity and hole points for each grid. This code was developed by Meakin [3] and it uses an innovative inverse mapping of the computational space to compute hole and outer boundary interpolation stencils with minimal search time. The major expense in DCF3D is the creation of the inverse maps. However, these maps are independent of the relative orientation of each grid so the same mappings can be used repeatedly during the grid motion. The DCF3D code dynamically updates the intergrid connectivities and hole points and is called as a subroutine to the OVERFLOW CFD solver.

Blade Motion

The method assumes rigid blade motions in flap and pitch. The complex blade motion due to aeroelastic deformation is not currently included, however it is a straightforward modification to the method described below [13]. The periodic blade motion for pitch and flap as a function of blade azimuthal angle, ψ, can be described by a the first three terms of a Fourier series as shown in Eqs. (1) and (2).

Pitch

$$\theta = \theta_o + \theta_{1c}\cos\psi + \theta_{1s}\sin\psi \qquad (1)$$

Flap

$$\beta = \beta_o + \beta_{1c}\cos\psi + \beta_{1s}\sin\psi \qquad (2)$$

For the general case, lag motions and shaft tilt are also included in the specified blade motions, however, these are not necessary for the test cases for this paper since they consist of two-bladed teetering rotors with zero shaft tilt.

The flow solver uses Eulerian angles to implement these blade motions in a fixed inertial reference frame. At each time step, the blade rotates by an increment of $\Delta\psi$ that results in changes in pitch and flap. These incremental changes in blade position are imposed by transforming the most current blade surface vectors to new locations through successive matrix multiplications as shown in Eq. (3).

$$T = [A]\,[B]\,[C]$$
$$\vec{x}_{new} = T\vec{x}_{old} \qquad (3)$$

The transformation matrix T consists of the rotation matrices A, B, and C. These matrices represent the three coordinate rotations and are described by Amirouche [14].

Pressure and Pressure Derivative Interpolations

The OVERFLOW code was modified to compute the pressure field and the pressure derivatives at all the grid-points and then interpolate the resulting information onto the Kirchhoff surfaces for postprocessing. At each point in the field the static pressure is computed from the density, mass flux and total energy as shown in Eq. (4).

$$P = \rho(\gamma - 1)\left[e - \frac{1}{2}\left(u^2 + v^2 + w^2\right)\right] \qquad (4)$$

where P is the pressure, ρ is the density, e is the internal energy, u,v and w are the Cartesian velocities and γ is the ratio of specific heats. The temporal derivative of the pressure, $\partial P/\partial t$, is then converted from the rotating coordinate frame to the inertial frame using the chain rule and grid metric terms as developed in Ref. [5]. The three components of the pressure gradient are also computed using the chain rule and the grid metrics from the flow solver.

In order to perform the Kirchhoff interpolations, the method uses the overset grid connectivity information from the flow solver. The nonrotating Kirchhoff surface is simply treated as another intergrid boundary surface that receives flow information and the pressure information.

During the flow solution process, the method stores a large quantity of data to disk for postprocessing. At every 5 degrees of rotation, the blade geometry, flowfield conserved variables, pressure, pressure gradient and various other post processing information are stored for all of the grids. At one degree increments, the solver saves the pressure information for the nonrotating Kirchhoff surface to a separate file. The resulting Kirchhoff surfaces files are then postprocessed to compute the far-field acoustic signature.

Kirchhoff Acoustics Method

It is not practical to continue the CFD solution to large distances from the rotor blade. Large numbers of mesh points are required and the calculation rapidly becomes too large for existing computers. An alternate approach is to place a nonrotating Kirchhoff surface around the rotor blades as shown in Figure 1. A rotating-surface formulation such as that described in Refs. [5,15] could also be used, however the nonrotating method avoids the problems associated with supersonic motion of the Kirchhoff surface for high-speed cases.It

The Kirchhoff surface translates with the rotor hub when the helicopter is in forward flight. The acoustic pressure, p, at a fixed observer location, $\vec{x}$, and observer time, t, is determined from the following integration on the cylindrical surface:

This formulation is taken from Farassat and Myers[16]. It assumes that the Kirchhoff surface is moving with Mach number $\vec{M}$. The distance between a point on the Kirchhoff surface and the observer is given by $|\vec{r}|$. Also note that the entire integral in Eq. (5) is evaluated at the time of emission for the acoustic signal, τ.

$$p(\vec{x}, t) = \frac{1}{4\pi}\int_S \left\{\frac{E_1}{|\vec{r}|(1 - M_r)} + \frac{E_2 p}{r^2(1 - M_r)}\right\}_\tau dS \qquad (5)$$

The expressions for E_1 and E_2 are given as:

$$E_1 = \left(M_n^2 - 1\right)p_n + M_n\vec{M}_t \bullet \nabla_2 p - \left[\frac{M_n p_t}{a_\infty}\right] - \left[\frac{(\cos\theta - M_n)\,p_t}{a_\infty(1 - M_r)}\right] \qquad (6)$$

$$E_2 = \left[\frac{1 - M^2}{(1 - M_r)^2}\right](\cos\theta - M_n) \qquad (7)$$

These expressions assume that the surface is moving with steady translational motion. Additional terms required to account for unsteady and/or rotational motion are given by Farassat and Myers [16].

In the above equations, M_n and M_r are the components of $\vec{M}$ normal to the Kirchhoff surface and in the direction of the observer. $\vec{M}_t$ is the velocity vector tangent to the Kirchhoff surface, and $\nabla_2 p$ is the gradient of the pressure on the Kirchhoff surface. The freestream speed of sound is assumed to be uniform at a_∞, and the angle, θ, is the angle between the normal to the Kirchhoff surface and the far-field observer.

Evaluation of the acoustic pressure at an observer time, t, requires that the integrand in Eq. (5) be evaluated at a different time of emission, τ, for each differential area

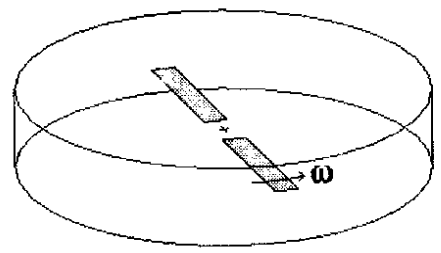

Figure 1: Nonrotating Kirchhoff surface for a helicopter rotor blade.

element on the Kirchhoff surface. This requires two interpolations. First, the overset-grid flow solver performs a spatial interpolation of pressure and pressure derivatives directly onto the Kirchhoff surface at each time step using DCF3D as described above. The DCF3D interpolations onto the Kirchhoff grid are very efficient and do not significantly increase the overall computational cost. Second, a temporal interpolation is then performed in the Kirchhoff- surface database. For each evaluation of the integrand in Eq. (5), the appropriate value of emission time is determined by noting that the time delay between the emission of the signal and the instant that it reaches the observer is equal to the distance that the sound must travel divided by the freestream speed of sound. This formulation leads to a quadratic equation for the time of emission, τ. Further details are given in Refs. [5,6]. Once the emission time has been determined, the appropriate pressure and pressure derivative values for Eqs. (5-7) are retrieved using linear temporal interpolation in the stored Kirchhoff-surface database.

The Kirchhoff surface consists of a top, bottom and side meshes as shown in Fig. 1. Each of these meshes contains 43,200 data points for a total of 129,600 grid points. The top and bottom surfaces are located approximately 1.5 chord lengths above and below the plane of the rotor blade. The side mesh is located approximately two chords beyond the tip of the blades. The resulting Kirchhoff surface is tilted for lifting cases to match the rotor tip path plane. The pressure data on the Kirchhoff surface is stored at intervals of one degree azimuthal angle. References [5,6] show that these Kirchhoff surface locations and temporal storage intervals are appropriate for the types of HSI and BVI noise that are modeled in this paper.

Test Cases for Aeroacoustic Simulation

HSI and BVI Cases

We have chosen two test cases for demonstration of our helicopter aeroacoustics prediction scheme. The first case simulates the high-speed impulsive (HSI) noise experiment of Schmitz et al. [17]. In this experiment, acoustic signals were recorded from a 1/7 scale model of the Army's AH-1 OLS helicopter main rotor. These OLS rotor blades are rectangular with 8.2° of twist from root to tip. The thickness-to-chord ratio is 0.0971 and the blades have a pre-cone angle of 0.5°. The rotor radius, R, is equal to 9.22 chordlengths with a blade root cutout at 0.182 R.

Our HSI test case has a hover-tip Mach number equal to 0.664, an advance ratio of 0.258 and a rotor thrust coefficient of 0.0054. The rotor has zero shaft tilt, but its tip path plane is tilted forward 3.25° by controlling the longitudinal flapping motion.

In spite of the fact that the HSI model rotor experiment has a significant amount of thrust, the CFD computations in previous analyses have computed rotor blade configurations that are untwisted and nonlifting. The nonlifting assumption simplifies the problem because the rotor wake for a nonlifting blade has a minimal influence on the blade aerodynamics and acoustics. The justification for neglecting the rotor thrust is that HSI pressure signals in the plane of the rotor are generally insensitive to thrust. This approximation has been experimentally documented (to first order) by Schmitz et al. [17].

The nonlifting approximation is not necessary in our Navier-Stokes/Kirchhoff method, since the flow solver captures the rotor wake system as part of the overall solution. Thus we have modeled this case as a lifting rotor with prescribed blade motions. In addition, we have also computed the nonlifting configuration so that we can compare our results to previously-published computations [5,6].

Our second demonstration case is a blade vortex interaction (BVI) noise simulation that was experimentally tested by Splettstoesser et al. [18]. These experiments also used the 1/7 scale model AH-1 OLS rotor system described above. The aerodynamic conditions are set to a hover-tip Mach number of 0.664, an advance ratio of 0.164, and a thrust coefficient of 0.0054. The shaft angle is 0°, however the rotor tip-path plane is tilted back by 1° using longitudinal flap control. These flow conditons produce both advancing and retreating-side BVI events plus advancing side unsteady transonic flow. Accurate numerical resolution of the rotor wake system is very important since the tip vortices have a strong influence on the unsteady aerodynamics and acoustics.

Our numerical simulations require that the complete rigid blade motions in Eqs. (1) and (2) be specified as input to the flow solver. This causes problems because not all of the motion coeffients are available from the experimental data. Typically, a few blade control settings are held fixed during the experiment and others are adjusted to trim the rotor and match a predetermined thrust. We could also iteratively adjust the control settings to trim the rotor in our CFD calculation, but this would require additional computer time. For instance, three trim iterations would increase our overall computer time be a factor of three.

In order to minimize the computational time, we chose to estimate reasonable blade motion coefficients in Eqs. (1,2) from either experimental run logs or from an approximate blade-trim analysis. The resulting blade motion should be close to a trimmed solution. We can check the degree to which the rotor is trimmed by comparing the computed thrust to the experimental values and checking for zero rolling moments over the rotor disk.

Table 1: Blade motion coefficients.

	θ_0	θ_{1c}	θ_{1s}	β_0*	β_{1c}*	β_{1s}*
HSI	7.66	1.0	-7.72	0.5	3.25	0.0
BVI	5.39	-1.88	-1.85	0.5	-1.0	0.0

Table 1 shows the blade motion coefficients that we used for the HSI and BVI test cases. The coefficients for the HSI case were obtained from a solution to the rotor trim equations in Ref. [19]. The coefficients for the BVI case are measured values taken from the original experimental run logs. The starred coefficients in Table 1 are fixed control inputs that are specified in the experiment. All blade pitch angles are specified for the 75% radial location.

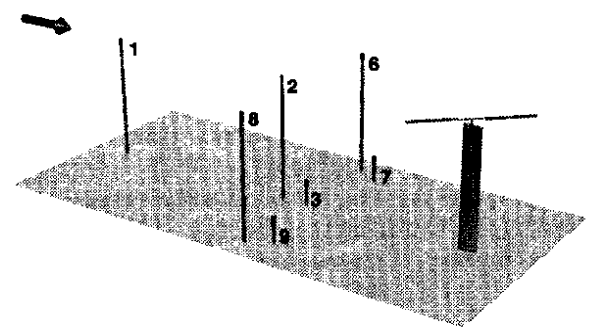

Figure 2: OLS Rotor acoustic microphone locations in wind tunnel.

Figure 2 shows the locations of the experimental microphones for both the HSI and BVI experimental test cases. The rotor moves in a counterclockwise direction which means that microphones (8,9) and (6,7) are located on the retreating and advancing sides respectively. More precise microphone locations are given in Table 2 below. The origin for these coordinates is the rotor hub, with +x aligned with the tunnel freestream, +y toward the 90° azimuthal direction and +z pointing above the plane of the rotor.

OLS Blade Grid System

The aeroacoustic overset grid system for the AH-1 OLS model rotor consists of 4 overset computational grids plus the Kirchhoff surface which was described earlier. This grid system is highlighted in Fig. 3. The computational grids consist of one near-field grid for each rotor blade, an intermediate grid to convect the rotor near-wake system and a global background mesh to convect the far wake and implement the far-field boundary conditions.

Table 2: Experimental microphone locations

Mic	x	y	z
1	-63.43	0.0	0.0
2	-31.717	0.0	0.0
3	-27.467	0.0	-15.858
6	-27.467	15.858	0.0
7	-23.787	13.733	-15.858
8	-27.467	-15.858	0.0
9	-23.787	-13.733	-15.858

The rotor blade grids are C-H topology with clustering near the blade tip, root, leading and trailing edges. These grids consist of 123x57x51 points in the chordwise, spanwise and normal directions respectively. There are 95 points on the blade surface in the chordwise direction and 26 points in the spanwise direction. Beyond the blade root and tip sections, the C-H surface grid collapses to a zero-thickness slit. The hyperbolic grid generator by Chan et. al [20] was used to generate the blade volume grids.

The blade grids lie within a Cartesian intermediate grid with points concentrated in the vicinity of the blade. This intermediate grid rotates with the blades and extends approximately 3 chord lengths beyond the rotor blade tips, above and below the rotor plane. The intermediate grid consists of 71x71x45 points in the chordwise, spanwise and normal directions respectively.

The global background grid completes the overset grid system with 71x75x57 points. This background grid extends to 4 rotor radii from the hub center upstream,

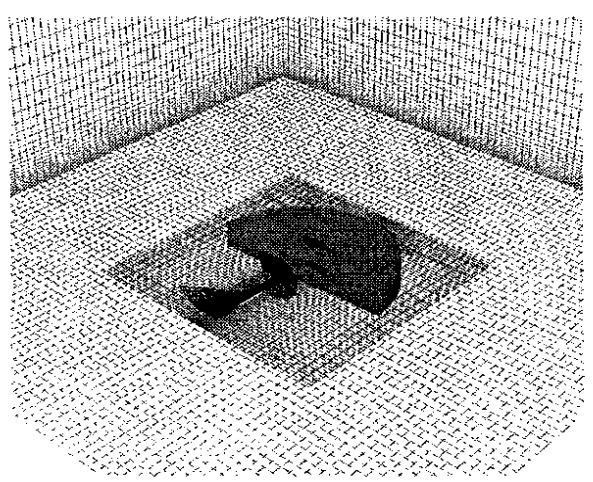

a) Background, intermediate and acoustic grids.

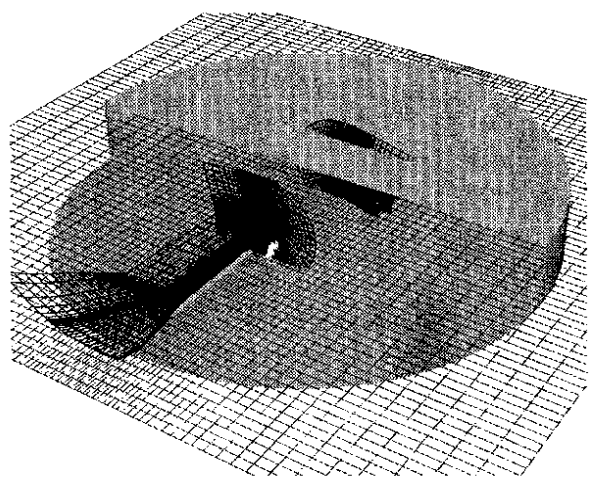

b) Kirchoff surfaces, intermediate and blade grid.

Figure 3: Aerodynamic and acoustic overset grid system for OLS rotor.

downstream, and to the sides. The grid also extends 2 rotor radii above the blade and 2.5 radii below.

The entire moving overset system totals roughly 1.25 million grid points. During the grid motions, the background grid remains stationary as the rotor blade and intermediate grids rotate through it. The intermediate grid is not affected by rotor blade motion, but the rotor-blade grids pitch and flap according to Eqs. (1) and (2). During their pitch and flap motions, the blade grids dynamically create holes within the intermediate grid while the intermediate grid creates holes within the background grid. Pressure information from either the rotor blade or intermediate grids is interpolated to the Kirchhoff surface.

Computer Implementation for the Two Test Cases

Both the HSI and BVI test cases use the grid system described above. This means that both simulations require the same amount of computer resources for each time step of the flow solver. Note that the background grid is very coarse, with uniform spacings of approximately 0.25 blade chord lengths. This grid is too coarse to accurately convect the rotor wake system, so we do not expect to see particularly good results for the BVI noise.

With this grid system (1.25 million total mesh points), the OVERFLOW code requires 20 seconds per time step on one processor of the Cray C-90. The time-accurate calculation impulsively starts from freestream conditions with the viscous no-slip boundary condition applied at the blade surfaces. The nonlifting HSI noise case requires one half revolution to eliminate the transient effects from this impulsive start. Afterwards, the complete solution can be computed in an additional one half revolution and stored for postprocessing. As mentioned before, the interpolation of pressure data onto the Kirchhoff surface does not significantly increase the total computation time. With a typical time step of 0.25 degrees of azimuthal angle, the total time for this calculation is 8 Cray C-90 hours.

The lifting HSI and BVI noise computations require at least two blade revolutions to eliminate the transient starting conditions. This longer start-up period for the lifting case is a result of additional unsteadiness of the rotor wake system. With a typical time step of 0.25 degrees of azimuthal angle, the total time for each calculation is about 16 Cray C-90 hours.

One aspect of these unsteady rotor calculations is that they produce a very large amount of output data. Our calculations store the complete solution for all 1.25 million grid points at 5 degree azimuthal intervals. The pressure and pressure gradients on the Kirchhoff surface are stored at one degree intervals. Additional postprocessing information for force, moment and blade surface pressures are also stored at 5 degree intervals. Because these files are so large, they must be moved onto an auxiliary storage device after each half revolution. The total amount of stored data per rotor revolution is approximately 13GBytes.

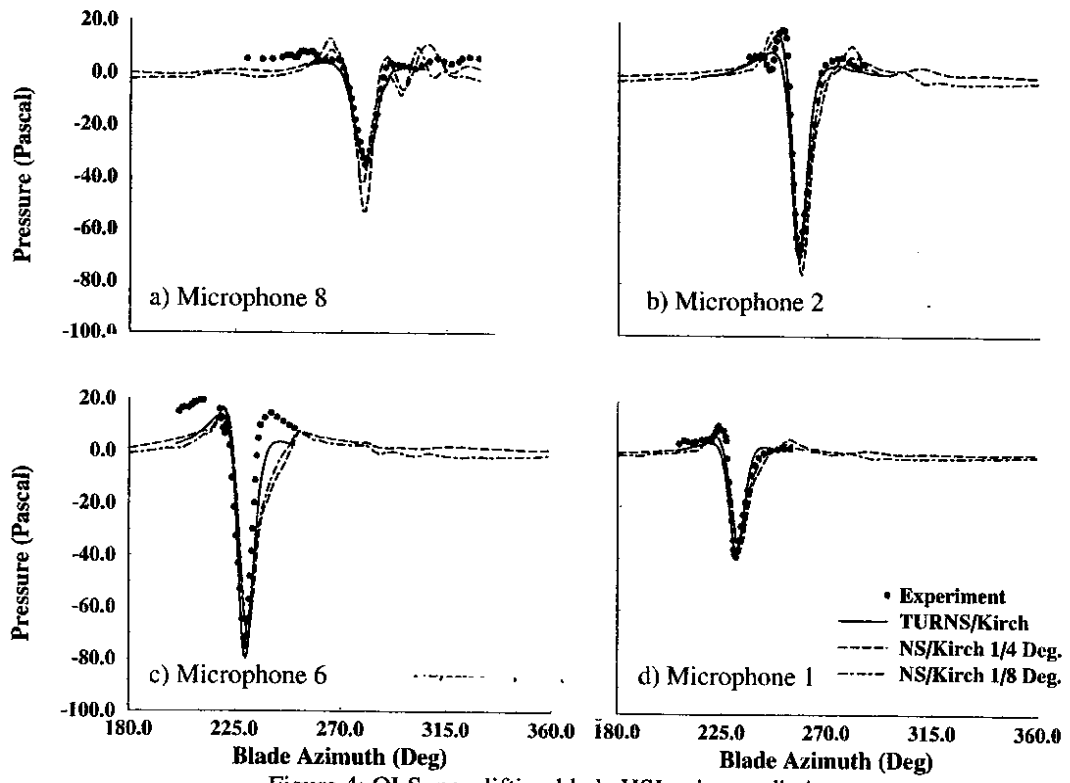

Figure 4: OLS, non-lifting blade HSI noise predictions
M_t= 0.665, μ=0.258.

Once these files are moved to auxiliary storage, they are later retrieved for visualization and acoustics postprocessing. Visualization of these large datasets requires a dedicated Convex computer system that is part of the Time-Accurate Visualization System (TAVS) at NASA Ames Research Center. The pressure data required by the Kirchhoff integration is retrieved to the Cray C-90 where it is split into six different pieces for the Kirchhoff program. The Kirchhoff integration computes the acoustic pressure contributions separately from each piece of the surface in order to reduce the total in-core memory requirements. These pressure contributions are later summed to determine the total far-field observer pressures. Alternatively, the Kirchhoff integrations can also be performed on the IBM SP-2 parallel computer as described in Ref. [7]. The parallel Kirchhoff code exhibits greater than 98% theoretical speedup on 80 processors of the SP-2.

On the Cray C-90, the Kirchhoff integration program requires 0.075 CPU seconds for each evaluation of pressure at an observer location in space, and an observer time, t. The Kirchhoff program runs at 470 MFLOPS on the Cray C-90 and the overall speed is approximately 20 times faster than the CPU times reported in Ref. [5]. The reason for this speedup is that the spatial interpolations onto the Kirchhoff surface are now computed by the flow solver, and not by the Kirchhoff integration program. The in-core memory requirement for the Kirchhoff code is 19MW. This cost could be further reduced by splitting the Kirchhoff surface up into smaller pieces and performing sequential integrations on each piece.

Results: Non-Lifting High-Speed Impulsive Noise

Computed acoustic pressures for the HSI case are compared in Fig. 4 to the experimental data for several different in-plane far-field microphones. The microphone numbers in this figure correspond to those used in Refs. [17,18] and are shown in Fig. 2. Also shown in this figure are computed results from the TURNS/Kirchhoff analysis in Ref. [5]. Two different timesteps were used in the OVERFLOW/Kirchhoff (NS/Kirchhoff) computations and Fig. 4 shows results from each. The first is equivalent to 0.25° of azimuthal angle per timestep and the second is equivalent to 0.125° timesteps.

All of the computations show excellent agreement with the experimental microphone data. The only significant differences between the computed results occur for microphone 8 on the retreating side of the rotor disk. Ref. [8] shows that the acoustic signal at this microphone location originates from the second quadrant of the rotor disk where the transonic unsteadiness is highest. It is not surprising that the maximum discrepancies in results between flow solvers and timestep modifications show up at this microphone location.

Overall, this test case serves as an excellent validation of the new NS/Kirchhoff analysis. The new results show good agreement with the previous TURNS/Kirchhoff results, considering that the earlier TURNS results solved the Euler flowfield equations while the current results model the full Navier-Stokes equations.

An additional consideration is that the TURNS code used the LU-SGS left-hand side solver with three "Newton" sub-iterations per timestep. These subiterations reduce the factorization error in the LU-SGS operator and thus improve the time accuracy for the calculation. Our OVERFLOW results did not use the "Newton" subiterations and show only minor sensitivity to timestep changes at microphone 8. In order to reduce computer time for the remaining calculations, we chose to run them all with a time step of 0.25°. The BVI calculation should be even less sensitive to timestep changes than the HSI since it has less unsteady transonic flow.

Results: Lifting High-Speed Impulsive Noise

Figure 5 shows experimental and lifting NS/Kirchhoff computed results for the four in-plane microphones. Also reproduced here for comparison, are the nonlifting NS/Kirchhoff results from Fig. 4. The main effect of the blade motion and lift is to increase the peak negative pressures by 25 to 50% compared to the nonlifting results. The lifting NS/Kirchhoff pressures also do not return to zero before and after the main pressure pulse.

The cause of this zero offset is not known although we initially suspected that it may be caused by the fact that the wake system from the lifting rotor passes through the bottom of the Kirchhoff surface. The Kirchhoff integration in Eqs. (5-7) assumes a uniform flow through the Kirchhoff surface which is technically violated for lifting rotors. We tested this hypothesis by moving the Kirchhoff surface farther away from the rotor disk. The top and bottom of the original Kirchhoff surface was located 1.5 chordlengths (s/C = 1.5) from the rotor disk and the top and bottom of the new surface was 2.5 chordlengths (s/C = 2.5) from the rotor disk.

Figure 5 shows that the new Kirchhoff surface location had little effect on the computed results for peak negative pressure. It did however, increase the zero offset by a slight amount. This seems to disprove our hypothesis since one would expect the flow through the bottom of the Kirchhoff surface to be more uniform for s/C=2.5 than for s/C=1.5 since the rotor wake system rapidly dissipates in the coarse background mesh. As a result, the cause of the zero offsets for the lifting results in Fig. 5 remains a mystery.

Figure 6 shows computed and experimental results for the three out-of-plane microphones. Here the lifting results show much better agreement with the experimental data than the nonlifting results. This is to be expected since the noise contribution due to blade lift is typically more important out-of plane than in plane. The nonlifting computations do not model this blade loading noise and underpredict the peak acoustic pressures as expected. Figure 6 shows excellent agreement between the lifting NS/Kirchhoff and experimental peak negative pressures. The

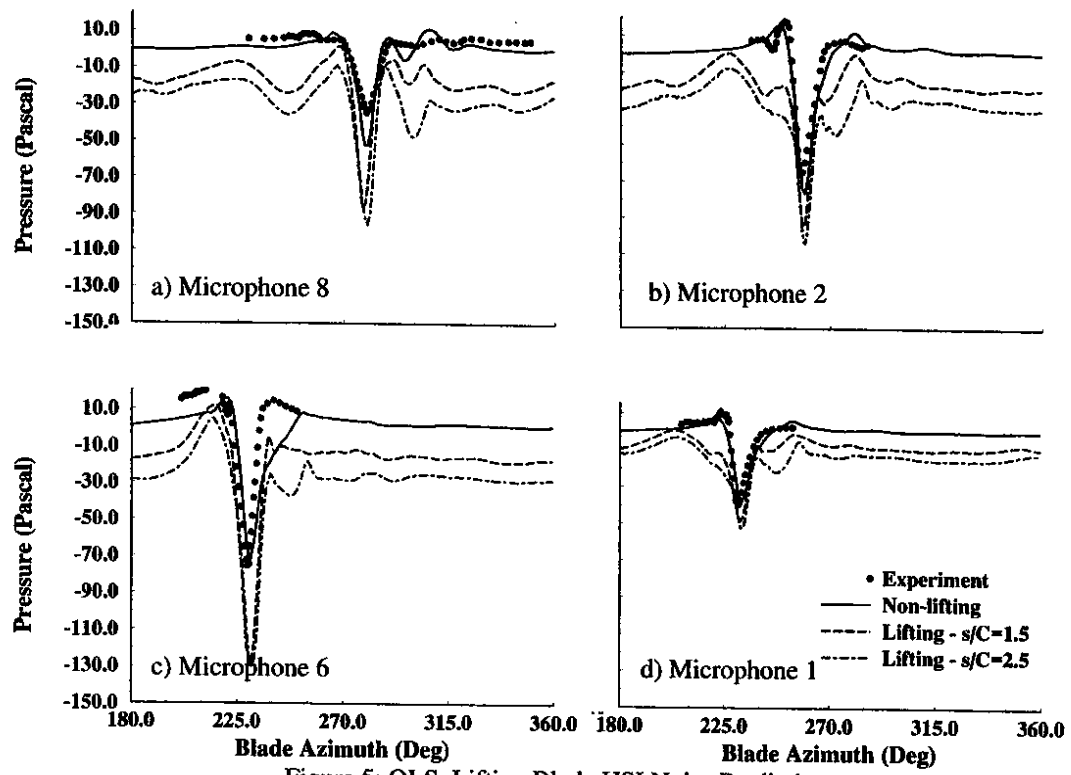

Figure 5: OLS, Lifting Blade HSI Noise Predictions
M_t= 0.665, μ=0.258

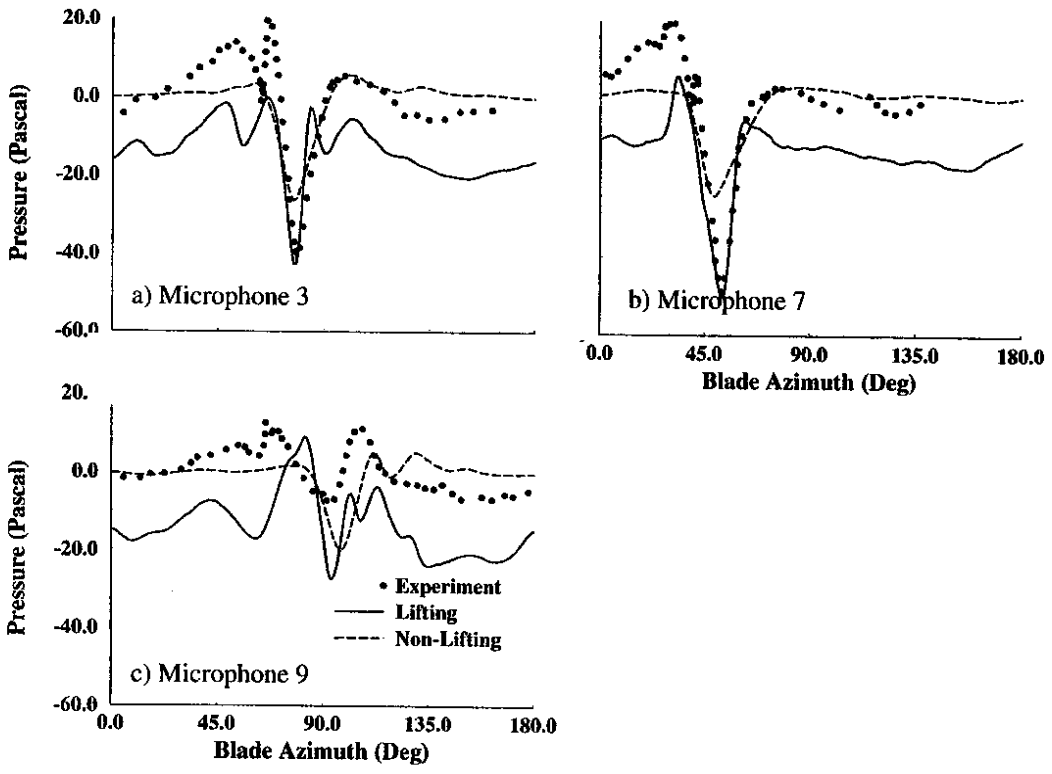

Figure 6: OLS, Lifting Blade HSI Noise Predictions
M_t= 0.665, μ=0.258

lifting NS/Kirchhoff results also show better agreement for the shapes of the acoustic signals than their nonlifting counterparts. The only problem with the lifting NS/Kirchhoff results is that the zero offset seen in Fig. 5 is also present in Fig. 6. This offset is not seen in the experimental data, nor in the nonlifting NS/Kirchhoff calculations.

Results: Blade-Vortex Interaction Noise

Computed and experimental results for the BVI case are shown in Fig. 7. The main discrepancy between the experimental and computed results is the zero pressure-offset problem that was also shown in Figs. 5 and 6. Aside from this problem, the computed and experimental results show similar trends for both in-plane and out-of-plane noise. For instance, the overall shapes of the experimental acoustic signals are reasonably-well predicted for in-plane microphone 2 and out-of-plane microphone 3 and 7. However, the predictions do not adequately show the rapid acoustic pressure fluctuations that result from blade-vortex interactions. This discrepancy results from the fact that the intermediate and background grids in the NS/Kirchhoff calculation are too coarse to convect the tip-vortices in the rotor wake without excessive dissipation.

Summary and Conclusions

This paper presents an overall framework to compute helicopter aerodynamics and acoustics. The key elements in this framework are the overset grid generation, the domain connectivity control (DCF3D), the Navier-Stokes flow solver (OVERFLOW), and the Kirchhoff acoustics integration. One way that this analysis differs from earlier work is that the rotor wake system is computed as an inherent component of the total flowfield. Once we specify the blade motion, the wake and surface aerodynamics are computed in a tightly-coupled manner. In addition, interpolation onto the nonrotating Kirchhoff surface is performed by the flow solver at a negligible additional cost. Finally, the overset-grid scheme offers a framework for including finite-element models for blade dynamics as discussed in Ref. [13].

Computed results for nonlifting HSI noise match earlier computations and experimental data quite well. The lifting HSI results show reasonable agreement with experimental data, however they contain a zero offset problem

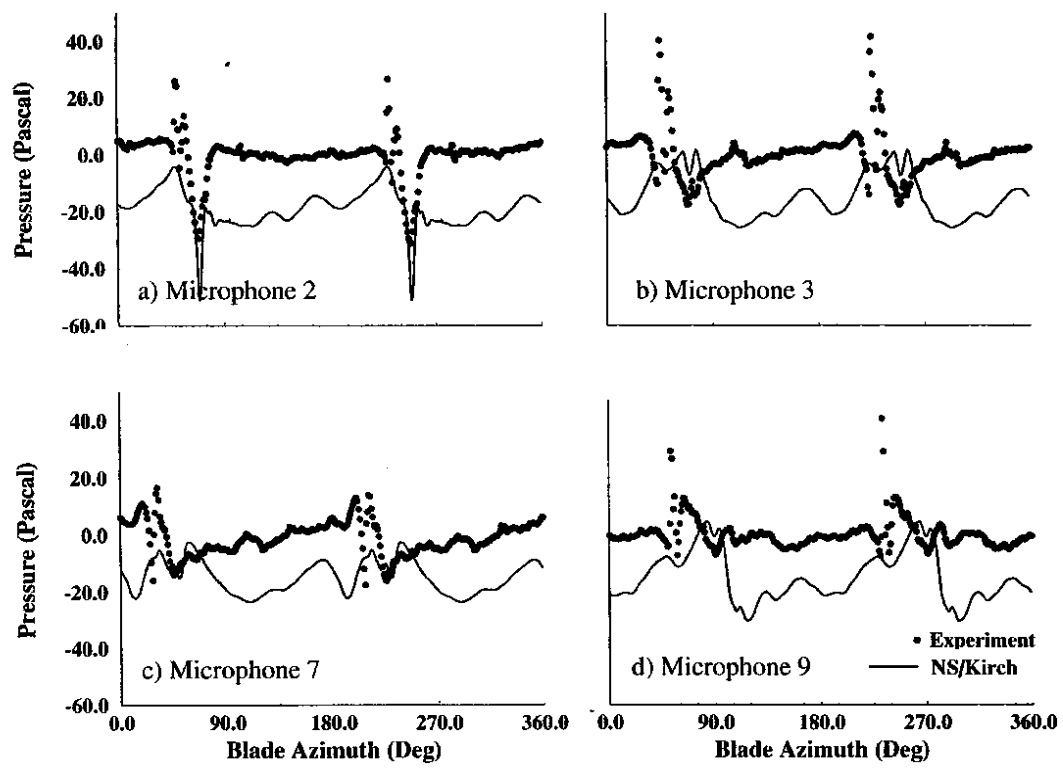

Figure 7: OLS lifting BVI predictions.
M_t= 0.664, μ=0.164

that is non-physical and whose cause is unknown. In spite of this problem, the lifting HSI predictions show much better agreement with the out of plane
experimental data than their nonlifting counterparts. Finally, the BVI noise predictions match the general shapes of the experimental acoustic data, but they exhibit a zero-offset problem and lack the rapid fluctuations in amplitude that are associated with BVI noise.

To put these results into perspective, the overall analysis has several key components, all of these must be functioning accurately in order to produce accurate far-field noise simulations. Results from the two test cases show that three areas in our analysis package need to be improved. First, we need to investigate the cause of the zero offset problem for the lifting-rotor acoustics predictions. Second, we need to improve the resolution in the intermediate and background meshes to convect the vortices in the rotor wake without excessive dissipation. We plan to increase the resolution in these grids for subsequent calculations and study the effects of these changes on the computed results. In addition, we plan to use higher-order spatial accuracy which will reduce the numerical dissipation for a given grid resolution. A final improvement requires the use of solution-adaptive grids in order to distribute grid points more efficiently in the rotor wake. This deficiency is being addressed with overset-grid compatible schemes such as the those proposed in Refs. [2,21,22].

The third area for improvement will address the time-accuracy in the flow solver. We plan to add Newton subiterations at each unsteady time step to the LU-SGS solution algorithm. These subiterations have worked well in the TURNS code [10] and should also be successful in OVERFLOW. We also plan to improve the unsteady solution algorithm from first to second order accurate in time.

In spite of the limitations discussed above, the methodology in this paper offers the potential for major improvements in our aeroacoustic prediction capability. Earlier methods based on comprehensive codes, lifting-line aerodynamics and the acoustic analogy have matured to a point where future fundamental improvements to these methods are unlikely. The main problem in these methods is the accurate simulation of the rotor wake system.

We don't claim to have solved the rotor wake problem yet, but our CFD-based aeroacoustics scheme offers a clear path to maximize the payoff from future improvements in CFD rotor-wake modeling. Any such improvements should immediately enhance our ability to compute helicopter and tiltrotor noise.

Acknowledgment

The authors appreciate the assistance of Franklin D. Harris in determining appropriate rotor motion coefficients for the lifting HSI test case.

References

[1]Ahmad, J.U., and Duque, E.P.N., "Helicopter Rotor Blade Computation in Unsteady Flows Using Moving Embedded Grids", AIAA Paper 94-1922, July 1994.

[2]Duque, E. P. N., Biswas, R., and Strawn, R. C., "A Solution-Adaptive Structured/Unstructured Overset Grid Flow Solver with Applications to Helicopter Rotor Flows," AIAA-95-1766, 13th AIAA Applied Aerodynamics Conf., San Diego, CA, June 19-21, 1995.

[3]Meakin, R., "Moving Body Overset Grid Methods for Complete Aircraft Tiltrotor Simulations," AIAA Paper 93-3350, 11th AIAA Computational Fluid Dynamics Conference, July 1993, Orlando, Florida.

[4]Duque, E. P. N., and Srinivasan, G. R., "Numerical Simulation of a Hovering Rotor Using Embedded Grids," Proceedings of the 48th AHS Annual Forum and Technology Display, Washington, DC, June 3-5, 1992.

[5]Strawn, R. C., Biswas, R., and Lyrintzis, A.S., "Helicopter Noise Predictions using Kirchhoff Methods", 51st Annual Forum of the American Helicopter Society, Fort Worth, TX, May 1995 (to appear in J. of Comp. Acoustics).

[6]Strawn, R. C., and Biswas, R., "Computation of Helicopter Rotor Acoustics in Forward Flight," Journal of the American Helicopter Society, Vol. 4, No. 3, July, 1995, pp. 66-72.

[7]Strawn, Roger C., Oliker, L, and Biswas, R., "New Computational Methods for the Prediction and Analysis of Helicopter Noise," AIAA96-1696, presented at the 2nd AIAA/CEAS Aeroacoustics Conf., State College, PA, 6-8 May, 1996 (submitted to the AIAA J. of Aircraft).

[8]Duque, E. P. N., Strawn, R. C., Ahmad, J., and Biswas, R., "An Overset Grid Navier-Stokes Kirchhoff-Surface Method for Rotorcraft Aeroacoustics Predictions," AIAA-96-0152, 34th AIAA Aerospace Sciences Mtg., Reno, NV, Jan. 15-18, 1996.

[9]Buning, P., Chan, Rieze, and Sondak, *OVERFLOW 1.6ap Users Manual*, Feb 1995.

[10]Srinivasan, G. R., Baeder, J. D., Obayashi, S., and McCroskey, W.J.,"Flowfield of a Lifting Rotor in Hover: Navier-Stokes Simulation," *AIAA Journal*, Vol. 30, No. 10, Oct. 1992, pp 2371-2378.

[11]Yoon, S. and Jameson, A., "An LU-SSOR Scheme for the Euler and Navier-Stokes Equations," AIAA Paper 87-0600, Jan, 1987.

[12]van Leer, B., Thomas, J.L., Roe, P.L. and Newsome, R.W., "A Comparison of Numerical Flux Formulas for the Euler and Navier-Stokes Equations," AIAA Paper 87-1104, June 1987.

[13]Ahmad, J.U., Bauchau O. and Duque, E.P.N., "Aeroelastic Prediction of a Helicopter Rotor in Forward Flight", Sixth International Symposium on Computational Fluid Dynamics, September 1995

[14]Amirouche, F.M.L., *Computational Methods in Multibody Dynamics*, Prentice Hall, 1992.

[15]Xue, Y., and Lyrintzis, A.S., "Rotating Kirchhoff Method for Three-Dimensional Transonic Blade Vortex Interaction Hover Noise," *AIAA Journal*, Vol. 32, No. 7, Jul. 1994, pp.1350-1359.

[16]Farassat, F., and Myers, M. K., "Extension of Kirchhoff's Formula to Radiation from Moving Surfaces," Journal of Sound and Vibration, Vol. 123, No. 3, 1988, pp. 451-460.

[17]Schmitz, F. H., Boxwell, D. A., Splettstoesser, W. R., and Schultz, K. J., "Model-Rotor High-Speed Impulsive Noise: Full-Scale Comparisons and Parametric Variations," Vertica, Vol. 8, No. 4, 1984, pp. 395-422.

[18]Splettstoesser, W. R., Schultz, K. J., Boxwell, D. A., and Schmitz, F. H., "Helicopter Model Rotor-Blade Vortex Interaction Impulsive Noise: Scalability and Parametric Variations" presented at the 10th European Rotorcraft Forum, The Hague, Netherlands, Aug. 28-31, 1984.

[19]Harris, F. D., "Rotary Wing Aerodynamics - Historical Perspective and Important Issues," presented at the 1987 AHS Specialists' Meeting on Aerodynamics and Aeroacoustics, Feb. 25-27, 1987.

[20]Chan, W.M., Chiu, I.T., and Buning. P.G., "User's Manual for the Hyperbolic Grid Generator and the HGUI Graphical User Interface," NASA TM 108791, October 1993.

[21]Meakin, R., L., "An Efficient Means of Adaptive Refinement Within Systems of Overset Grids," AIAA-95-1722, presented at the 12th AIAA Comp. Fluid Dynamics Conf., San Diego, CA, June 19-22, 1995.

[22]Ramachandran, K., Tung, C., and Caradonna, F. X., "Rotor Hover Performance Prediction Using a Free Wake CFD Method," Journal of Aircraft, Vol. 26, No. 12, December 1989, pp. 1105-1110.